JOURNAL OF MATERIALS SCIENCE 27 (1992) 2093–2100

# Fibre and fibre-surface treatment effects in carbon/aluminium metal matrix composites

A. P. DIWANJI*, I. W. HALL
*Materials Science Program, University of Delaware, Newark, DE 19716, USA*

A systematic study of the relationship between the microstructure of the interface in C/Al composites and its dependence on variations in squeeze-casting parameters has been undertaken. This research has shown that the amount of $Al_4C_3$ reaction product at the interface is dependent on the surface structure of the reinforcing fibre and the surface treatment of the fibre. Additionally, the interface shear strength increases with an increase in the amount of reaction product at the interface. An increase in interface shear strength leads to a decrease in composite longitudinal strength. High-resolution electron microscopy and X-ray photoelectron spectroscopy analyses indicate that carbide formation is a conventional two-step process of nucleation and growth . Nucleation occurs preferentially at graphite edge planes on the carbon fibre surface, and growth is restricted along certain matrix planes and directions.

## 1. Introduction

Carbon fibre-reinforced aluminium metal matrix composites are of great interest for aerospace and commercial applications because of their high strength-to-weight ratio and their potential for economical fabrication by squeeze casting or similar methods. However, as with all composite systems, the interface is of great importance [1, 2], and the reaction taking place at the carbon–aluminium interface at temperatures $> 500\,^{\circ}C$ to form aluminium carbide, $Al_4C_3$, has long been considered critical in affecting the strength of C/Al composites [3–8]. However, although several studies have been performed to evaluate the effects of reaction products on C/Al composite properties, the conclusions are apparently contradictory [3–12]. Wu [3], and Yoon and Okura [12], showed that the amount of $Al_4C_3$ increased with increasing thermal exposure times above 500 °C, and this increase was associated with a loss in tensile strength. Nayeb-Hashemi and Seyyedi [4] performed TEM studies of Gr/201Al composites and reported the presence of $Al_4C_3$ and $Al_4O_4C$ at the interface. They also concluded that an increase in the reaction zone reduced mechanical bonding considerably. Khan [9] showed that up to 500 °C, little degradation of strength occurred, while for composites exposed to higher temperatures the strength declined more significantly. Contrary to the above, Blankenburgs [10] found that the formation of $Al_4C_3$ was not necessarily detrimental. The carbide formed as small platelets at the interface and the tensile strength of the composites improved considerably after development of small amounts of carbide. However, further growth of the carbides by exposure at high temperature did not degrade the composite strength. Similarly, Harrigan [11] reported that long exposures at high temperatures neither significantly changed the interface nor degraded the strength of the composite. As will become clear later, some of the disparities in observed reaction effects are almost certainly due to the use of different fibres and matrices.

Therefore in order to understand the interaction between aluminium and carbon fibres, it is necessary to understand the microstructure, especially the surface structure of the carbon fibres. The structure of carbon fibres has been characterized by X-ray diffraction (XRD) and, generally, the greater the degree of preferred orientation of the graphite planes parallel to the fibre axis, the higher the tensile modulus [13, 14]. The surface is usually the most highly oriented part of the fibre, and consists of exposed edges of graphite planes as well as graphite basal planes. The graphite planes exposed on their edge have partially attached carbon atoms with high-energy $sp^2$ hybridized bonds, and consequently these carbon atoms eagerly chemisorb oxygen to form reactive radicals which are known to be important in adhesion in resin-based composites [15]. It has been suggested that these complexes also bond with the matrix metal [16]. The bases of the graphite planes expose carbon atoms that interact by the low-energy $\pi$-bonds, forming weaker bonds with the matrix metal at the fibre surface.

In addition to its chemical characteristics, the fibre surface has important topographical features and exhibits a more or less fibrillar microtexture, microporosity, cleavage cracks, crystallite boundaries, foreign inclusions or impurities and fracture-inducing flaws [15]. All of these features can affect the

* *Present address*: Lord Corporation, 1635 West 12th St., Erie, PA 16514, USA.

0022–2461  

fibre–matrix adhesion, and therefore, the fibre–matrix interface shear strength.

Despite the large body of information on interface reaction in C/Al composites, there has been little work on the effects of interfacial reaction on the interface shear strength and its consequences for tensile strength. There has to date been no systematic study of the relationship between the microstructure of the interface in C/Al composites and its dependence on systematic variations in squeeze-casting parameters. Furthermore, as mentioned above, the mechanism by which $Al_4C_3$ is formed at the interface is also imperfectly understood.

If the interface is to be tailored for the achievement of optimum mechanical properties, it is necessary to understand the nature of adhesion at the interface and its dependence on various processing/manufacturing parameters. Our recent research programme investigated the effects of many variables including type of carbon fibre, surface treatments of fibres, matrix alloy variation, fibre distribution, heat treatment, volume fraction, melt superheat and fibre preform temperature. Here we present the results of the variations in fibres and surface treatments on the interface in A356 aluminium alloy squeeze-cast metal matrix composites. Interest centres on the longitudinal mechanical properties and, in particular, the fibre–matrix adhesion and how it is affected by choice of fibre and surface treatment.

## 2. Experimental procedure

The composites investigated in this program were squeeze-cast by Honda R & D Co. Ltd, Wako-Shi, Japan. Preforms were made using tows of 6000 fibres and an acrylic resin binder to produce castings with 35 vol % of unidirectionally reinforcing fibres. For squeeze casting, the preform and melt temperatures were 600 and 780 °C, respectively, and an infiltration pressure of 70–100 MPa was used. Samples were prepared with high tensile T300-99 fibres and three types of high modulus fibre, P55, PMX and M40; the matrix was A356, a common casting alloy with 6–7.5 % Si, 0.3 % Mg and 0.3 % Fe. T300 and M40 are PAN-based fibres, and P55 and PMX are pitch-based fibres; all were obtained without sizing or surface treatment. These fibres were chosen because of their availability and good potential for commercial usage.

In addition to these composites, C/Al composites were prepared with anodic oxidation surface treatments applied to the M40 and T300 fibres, designated M40-90-1 and T300-90; respectively. The fibres were surface-treated by the fibre manufacturer, Toray Industries, Japan. This surface treatment involved anodically etching the fibres in dilute sodium hydroxide electrolyte for 1–2 min. Other M40 fibres, designated M40-90-2, were subjected to nitric acid surface treatment. In this case they were immersed in 1 N concentrated nitric acid for 96 h. Table I lists the properties of the fibres used.

Dog-bone samples with a gauge length of 25.4 mm and a cross-sectional area of 50 $mm^2$ were machined from the squeeze castings. The samples were tested in a 10-ton static Instron machine at room temperature at a strain rate of $5 \times 10^{-2}$ $min^{-1}$. Two strain gauges were attached to the gauge length of each sample.

Rectangular double-notched samples, as shown in Fig. 1, were machined from each of the castings and tested in compression so as to evaluate the composite shear strength, $\tau_{cs}$, which is defined as load divided by the projected area, (161 $mm^2$). The sample geometry is similar to that recommended by ASTM D3846-79 [17], for the shear testing of polymer composites. Although, of course, the shear test used here does not measure the interfacial shear strength (ISS) directly, the ISS must be proportional to the measured composite shear strength, as the composite shear strength is a combination of matrix shear strength and ISS. SEM observations confirm that the failure occurs along the interface and not in the fibre. Therefore it is possible to make an estimate of the ISS from the measured composite shear strength using simple rule-of-mixtures calculations, as follows.

In the plane of rupture, the load in the shear test is simultaneously shared by the interface and the matrix between adjoining fibres. It is assumed that the strain is uniform in the direction perpendicular to the plane of rupture; this is a typical isostrain condition where the net shear strain of the plane of rupture is equal to the shear strain of the interface and the matrix. The plane of fracture in these shear test samples is not strictly flat, since the interface has the curvature of the fibre surface. It is assumed that the fibre area fraction in the plane of rupture is equal to the fibre volume fraction and, not unreasonably in view of the later fractography, that fibre/matrix interfacial shear produces semicylindrical surfaces on the fracture surface while matrix shear produces flat regions. Using the

TABLE I Details of fibre properties.

| Fibre type | Fibre diameter (μm) | UTS (MPa) | Young's modulus (GPa) | Failure strain (%) |
|---|---|---|---|---|
| M40 | 8–10 | 3000 | 430 | 0.65 |
| P55 | 8–10 | 1880 | 380 | 0.5 |
| PMX | 10–12 | 1700 | 370 | 0.5 |
| T300-99 | 10–12 | 3300 | 232 | 1.4 |
| M40-90-1 | 8–10 | 3000 | 430 | 0.5 |
| M40-90-2 | 8–10 | 2700 | 430 | 0.5 |
| T300-90 | 10–12 | 3300 | 232 | 1.4 |

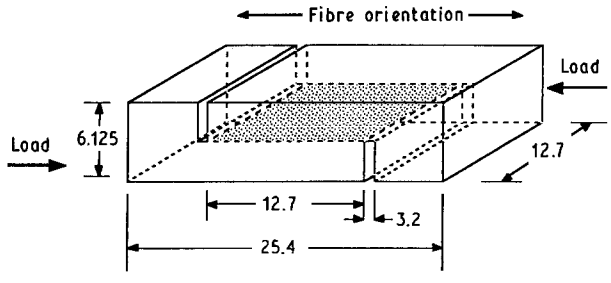


*Figure 1* Specimen geometry for composite shear-strength tests.

rule-of-mixtures, the measured composite shear strength in the plane of rupture can then be related to the ISS and the matrix shear strength by the following equation:

$$\left[\frac{\pi}{2}V_f + (1 - V_f)\right]\tau_{cs} = \left[\frac{\pi}{2}V_f\right]^2 \tau_{int} + [1 - V_f]^2\tau_m$$

where $V_f$ is the volume fraction of fibres, $\tau_{cs}$ is the measured composite shear strength, $\tau_{int}$ is the interface shear stress, and $\tau_m$ is the matrix shear stress. Inserting $V_f = 0.35$, $\tau_m = 45$ MPa (for the matrix alloy) and the $\tau_{cs}$ values into the above equation, $\tau_{int}$ for each type of composite can be estimated. These values are obviously only approximate and could be considerably refined by the use of stereological measurements, but as the shear fracture surfaces showed no gross differences, the results reflect trends in ISS.

Extensive transmission electron microscope (TEM) analysis of each of these composites has been carried out in order to characterize the fibre–matrix interface. Discs for TEM were mechanically thinned down to 100 μm, dimpled to 15 μm in the centre and then ion-milled to electron transparency on the cold stage of a Gatan Duo-Mill. X-ray photoelectron spectroscopy (XPS) has been carried out on each of the different kinds of fibres before infiltration in order to characterize the surface composition. The specific surface area of the fibres was determined by krypton adsorption and the amount of carbide was determined by methane generation.

## 3. Results

### 3.1. Carbon fibre variation

The results of the tensile and shear tests performed on the composites with alloy A356 as matrix and different types of carbon fibres as reinforcements are presented in Table II along with the calculated values for the rule of mixtures. Each data point is the average of at least five tests. Representative fractographs are presented in Section 3.4 below

M40/A356 samples did not fail in a pure tensile mode during testing. The failure mode was of the type termed non-catastrophic, indicative of a very low shear strength for the fibre–matrix interface and the fibres failed in order of weakness as dictated by the Weibull distribution function. The average composite shear strength of M40/A356 composites was 26 MPa.

A striking observation from Table II is that the tensile strengths decreased from sample 1 to sample 4, whereas the composite shear strength increased in that same order. Since the composite shear strength obtained from the shear test is proportional to the longitudinal shear strength of the interface as outlined above, the implication is that a higher interface shear strength leads to a lower tensile strength. This confirms the modelling results of several authors [1, 2, 18, 19]. It should be noted from Table II that, other than sample 1, all the other composites failed in the gauge length. The composite shear strength of M40/A356 was also almost half that of P55/A356, which itself had the lowest composite shear strength among the other composites in Table II.

### 3.2. Effect of fibre surface treatment

The results of the tensile and shear tests performed on the composites with surface-treated and untreated M40 and T300 carbon fibres as reinforcements are presented in Table III along with the calculated values for the rule-of-mixtures. Again, each data point is the average of at least five tests.

It is noted that fibre surface treatment consistently led to a decrease in the average tensile strength and to an increase in the composite shear strength for both M40 and T300 fibres. Although the average properties of the surface-treated fibre composites were lower than the untreated fibre composites, there was considerably less scatter in the tensile data.

In all the above cases, there was no change in the fracture morphology of the shear specimens and fracture always proceeded along the fibre–matrix interface. As all the composites had the same nominal fibre volume fraction, the same alloy A356 as matrix, and fibre splitting was not observed, this is further confirmation that the changes in shear strength are directly related to changes in the interface.

Calculated values of ISS are given in Table IV and it is seen that surface treatment always increased ISS substantially, and sometimes dramatically. The ISS for M40 fibres increased from 40 MPa for untreated fibres to 234 MPa for nitric acid-treated fibres. Again, it is emphasized that although these are not true ISS values, they are believed to be representative of trends in the data.

TABLE II Mechanical properties of composites with different fibres as reinforcements.

| Sample | Composite type | UTS (MPa) | Young's modulus (GPa) | Failure mode | Composite shear strength (MPa) |
|---|---|---|---|---|---|
| 1 | M40/A356 | 856 (1167)[a] | 189 (197)[a] | Non-catastrophic | 26 |
| 2 | P55/A356 | 692 (775)[a] | 156 (178)[a] | Gauge length | 45 |
| 3 | PMX/A356 | 588 (712)[a] | 158 (175)[a] | Gauge length | 55 |
| 4 | T300-99/A356 | 461 (1272)[a] | 115 (127)[a] | Gauge length | 85 |

[a] Rule of mixtures values.

TABLE III Mechanical properties of composites with surface-treated fibres as reinforcements.

| Sample | Composite type | UTS (MPa) | Young's Modulus (GPa) | Failure mode | Composite shear strength (MPa) |
|---|---|---|---|---|---|
| 1 | M40/A356 Untreated | 856 (1167)[a] | 189 (197)[a] | Non-catastrophic | 26 |
| 5 | M40-90-1/A356 Anodic oxdn | 720 (1167)[a] | 190 (197)[a] | Gauge length | 49 |
| 6 | M40-90-2/A356 Nitric acid | 554 (1062)[a] | 191 (197)[a] | Gauge length | 75 |
| 4 | T300-99/A356 Untreated | 461 (1272)[a] | 115 (127)[a] | Gauge length | 85 |
| 7 | T300-90/A356 Anodic oxdn | 345 (1272)[a] | 113 (127)[a] | Gauge length | 100 |

[a] Rule-of-mixtures values.

### 3.3. Fibre surface analyses

Table V shows the fibre surface characteristics of the M40 fibres before and after surface treatment. The 96-h exposure of the fibre to 63 % $HNO_3$ led to at least a ten-fold increase in the specific surface area as compared to the untreated fibre. This treatment also led to a 10 % reduction in tensile strength which may be a contributory cause of the lower tensile strength of composites reinforced with these fibres. It is evident from the O/C ratios obtained by XPS that the nitric acid treatment led to a three-fold increase in the oxygen concentration on the fibre surface.

The anodic oxidation treatment for 2 min in concentrated NaOH was much less effective in increasing the specific surface area; however, longer treatment times can be expected to increase this effect. The XPS data show that the anodic oxidation treatment, which lasted only 2 min, is clearly more potent as an oxidizing treatment than the nitric acid treatment which lasted for 96 h.

TABLE IV Interface shear strengths calculated from the measured composite shear strengths.

| Composite type | $\tau_{comp.\ shear}$ (MPa) | $\tau_{interface}$ (MPa) |
|---|---|---|
| M40/A356 | 26 | 40 |
| P55/A356 | 45 | 116 |
| PMX/A356 | 55 | 155 |
| T300-99/A356 | 85 | 274 |
| M40-90-1/A356 | 49 | 131 |
| M40-90-2/A356 | 75 | 234 |
| T300-90/A356 | 100 | 334 |

TABLE V Surface characteristics of surface-treated fibres.

| M40 Fibre | UTS (MPa) | Specific surface area ($m^2\ g^{-1}$) | O/C (%) | $Al_4C_3$ (wt %) |
|---|---|---|---|---|
| Untreated | 3000 | 0.53 | 3.8 | 0.0072 |
| Anodic Oxidation | 3000 | 0.63 | 13.0 | 0.014 |
| Nitric acid | 2700 | 5.21 | 11.6 | 0.019 |

Finally, the amount of $Al_4C_3$ at the interface in the composites increased by at least a factor of two when the matrix was reinforced by surface-treated fibres.

### 3.4. Electron microscopy

As stated in Section 3.1 above, scanning electron microscopy of the fracture surface of M40/A356 samples confirmed that fracture had occurred by decohesion, leading to longitudinal shear failure at the interface and very extensive pull-out of the fibres, as shown in Fig. 2a. The T300, P55 and PMX composites all failed with a modest amount of pull-out in the cumulative mode—a typical such fractograph is shown in Fig. 2b. After any of the surface treatments, both M40 and T300 samples showed essentially flat fracture surfaces with almost no pull-out. Fig 2c shows such a typical surface, in this case an M40-90/A356 sample in which the fibres were nitric acid-treated before infiltration.

Similar clear trends emerged from the shear tests; untreated M40/A356 samples showed very clean fibres to which the matrix did not adhere well, while treated M40 fibres were much more strongly bonded, (Fig. 3a and b). Similarly, there was a greatly increased tendency for the matrix to adhere to the T300 fibre after surface treatment. Furthermore, the PMX and P55 fibres showed much debris adhering to the surface, (Fig. 3c).

TEM analysis of all the samples revealed that, overall there was excellent contact between matrix and fibre, and high resolution electron microscopy (HREM) failed to reveal any evidence for a general oxide layer. The only reaction product observed at the interface was $Al_4C_3$, which appears as needles in the TEM, the quantity depending upon the particular fibre and matrix under observation as detailed below. The silicon eutectic component was present throughout the matrix, and particularly at the interface. Other second-phase particles, such as $Al_8Mg_3FeSi_6$ and AlFeSi, were also frequently seen at the interface. These are normal products of solidification of cast aluminium alloys; they are not reaction products and are not believed to have any significant effects on the mechanical properties. The typical matrix structure

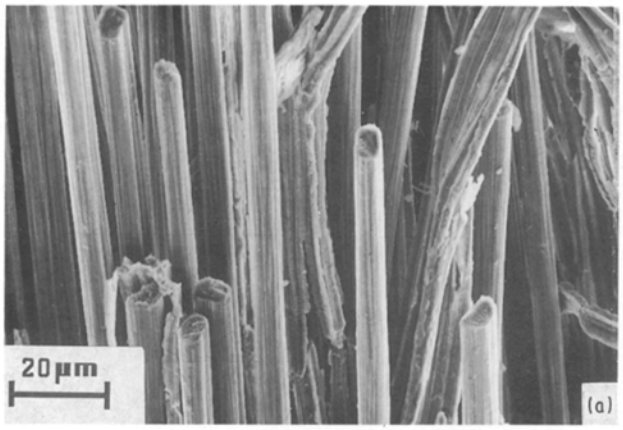


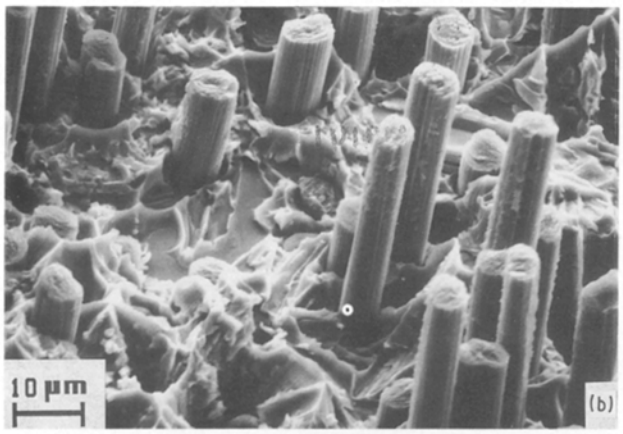


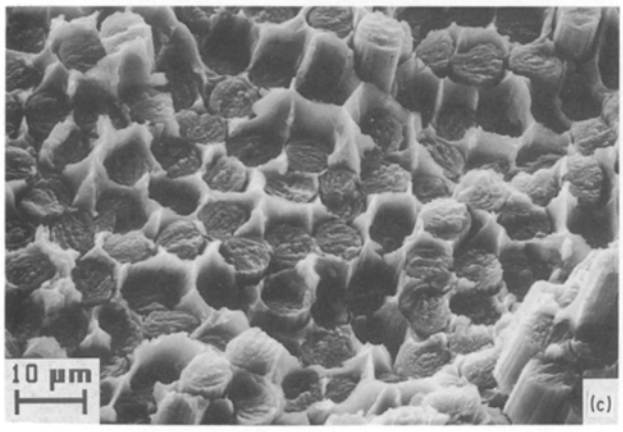


*Figure 2* (a) Tensile fracture surface of M40/A356 composite showing severe longitudinal shear and extensive fibre pull-out. (b) Tensile fracture surface of T300-99/A356 specimen showing modest pull-out length. (c) Fracture surface of M40-90/A356 composite (nitric acid surface-treated fibres) showing flat fracture surface without significant pull-out.

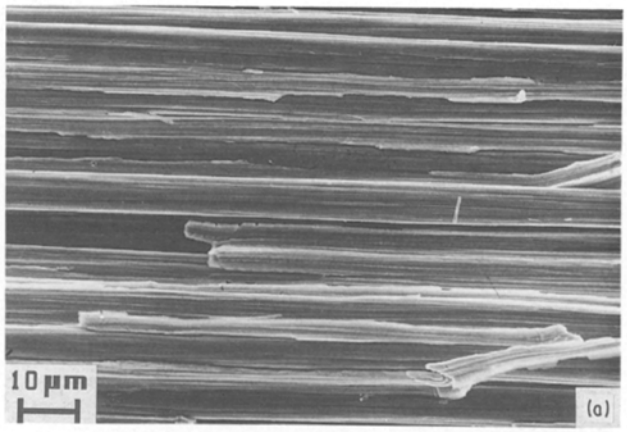


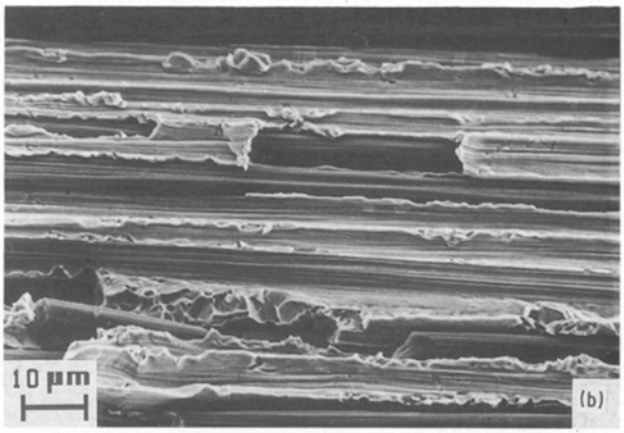


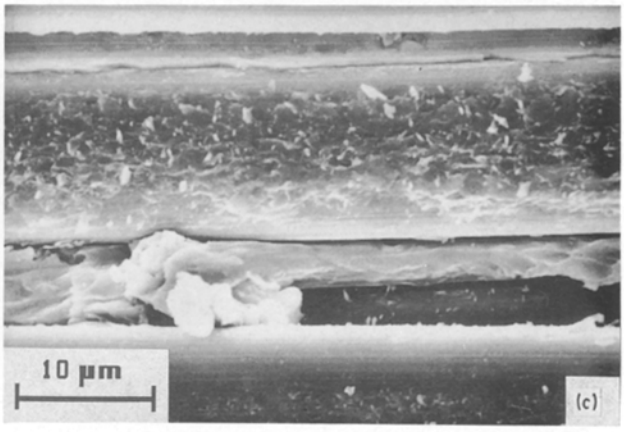


*Figure 3* (a) Shear fracture surface of untreated M40/A356 composite showing little adhesion between fibres and matrix. (b) Shear fracture surface of surface-treated M40/A356 composite showing improved fibre/matrix adhesion. (c) Shear fracture surface of PMX/A356 composite: debris adhering to the fibre surface indicates strong fibre/matrix adhesion.

consists of Si particles a few micrometres in diameter, small precipitates of $Mg_2Si$, and a high dislocation density.

The fibres exhibited increasing degrees of graphitization in the order T300, M40, P55 and PMX. The interfaces in P55/A356 and PMX/A356 were very similar in appearance. A transverse section of the fibre/matrix interface of a P55/A356 composite is shown in Fig. 4a, and the graphite planes are mainly seen to be arranged circumferentially around the fibre edge. In this case the planes extend several thousand nanometres, but the less highly graphitized fibres show a much reduced crystallite size and lower degree of orientation along the fibre axis. Fig. 4b shows a typical longitudinal section of the PMX/A356 interface. The fibres still show an obviously lamellar structure, and there is a large number of aluminium carbides at the interface.

Fig. 5a and b shows longitudinal sections containing the interface of T300-99 and T300-90 composites, untreated and surface-treated fibres, respectively. It is clear that surface treatment led to a greatly increased amount of carbide at the interface. Also, it can be seen that the degree of crystallinity in these fibres was much

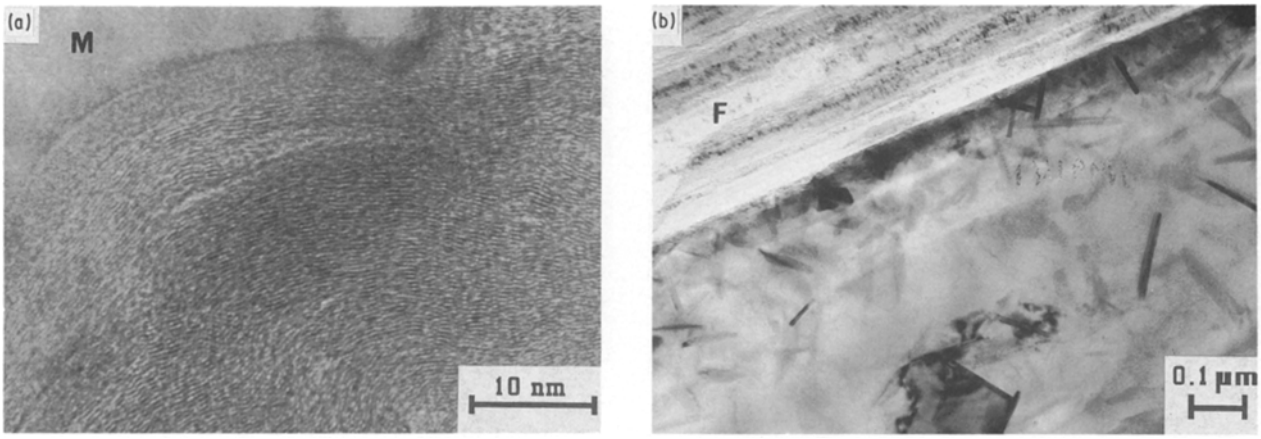


*Figure 4* (a) Transverse section of P55/A356 composite (matrix labelled M at top left): basal planes of the highly graphitized fibre are arranged circumferentially around fibre surface. (b) Longitudinal section of PMX/A356 composite showing fibre (marked F) at upper left and needle-like carbides at the interface.

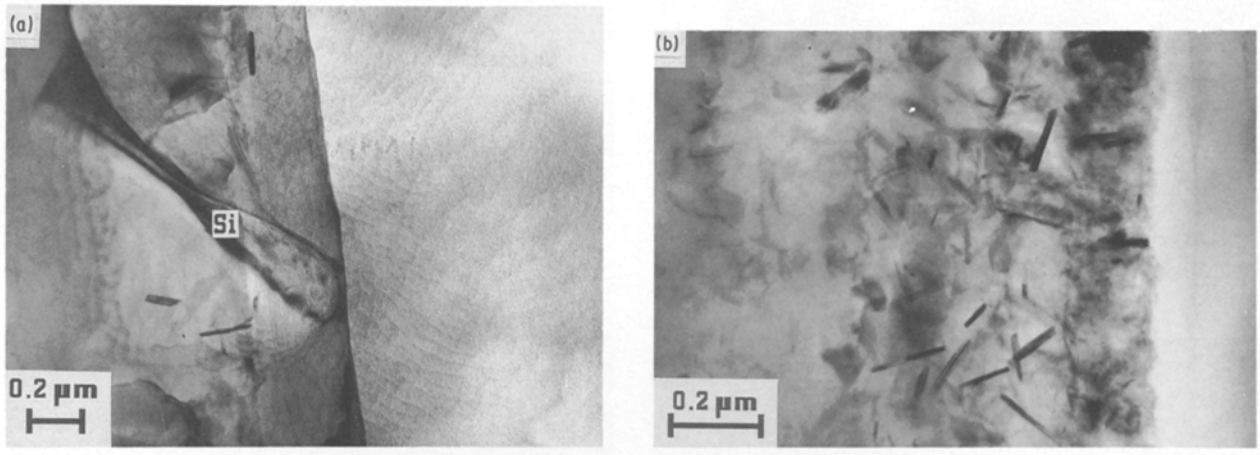


*Figure 5* (a) Longitudinal section of untreated T300-99/A356 composite showing occasional carbides and silicon (marked Si) at the fibre/matrix interface. (b) Longitudinal section of surface-treated T300-90/A356 composite showing very heavy precipitation of carbides at the fibre/matrix interface.

lower than in those illustrated in Fig. 4. Surface treatment led to a similar trend in M40 composites, and nitric acid treatment was found to lead to a greater carbide concentration than anodic oxidation.

The carbide/fibre interface was imaged by HREM in an attempt to elucidate the nature of the nucleation site. Clearly, the probability of identifying the exact location at which nucleation occurred is very small, but numerous micrographs indicate that there is frequently a direct correspondence between the edges of the graphite crystallites and the carbides. Fig. 6 shows approximate epitaxy between the (0 0 0 3) planes in an aluminium carbide and the (0 0 2) planes in the graphite. The carbide is almost parallel to the interface in this instance.

Diffraction pattern analysis showed that there was usually an orientation relationship between the carbide and aluminium matrix of the form

$$(0\,0\,0\,3)_{\text{carbide}} // (1\,1\,1)_{\text{Al}}$$

$$[1\,1\,\bar{2}\,0]_{\text{carbide}} // [1\,2\,\bar{3}]_{\text{Al}}$$

This orientation relationship is illustrated in Fig. 7a. Fig. 7b shows the corresponding micrograph in which a carbide has grown from an M40 fibre into the matrix and the small crystallite size is well illustrated. Note also that the graphite crystallites are considerably convoluted and present many sites at which the

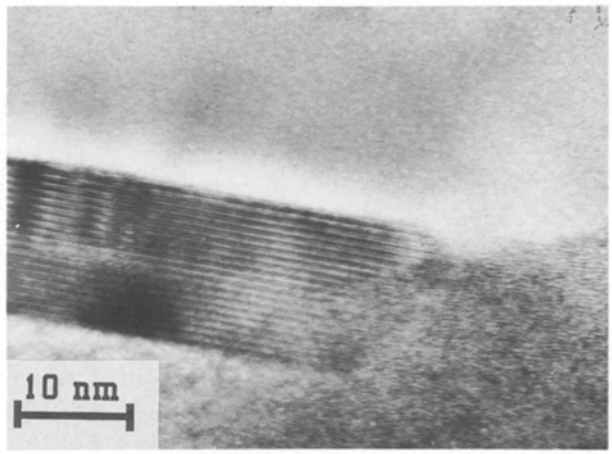


*Figure 6* Fibre/matrix interface in the PMX/A356 composite showing approximate epitaxy between $(0\,0\,0\,3)_{\text{carbide}}$ and $(0\,0\,2)_{\text{graphite}}$ planes.

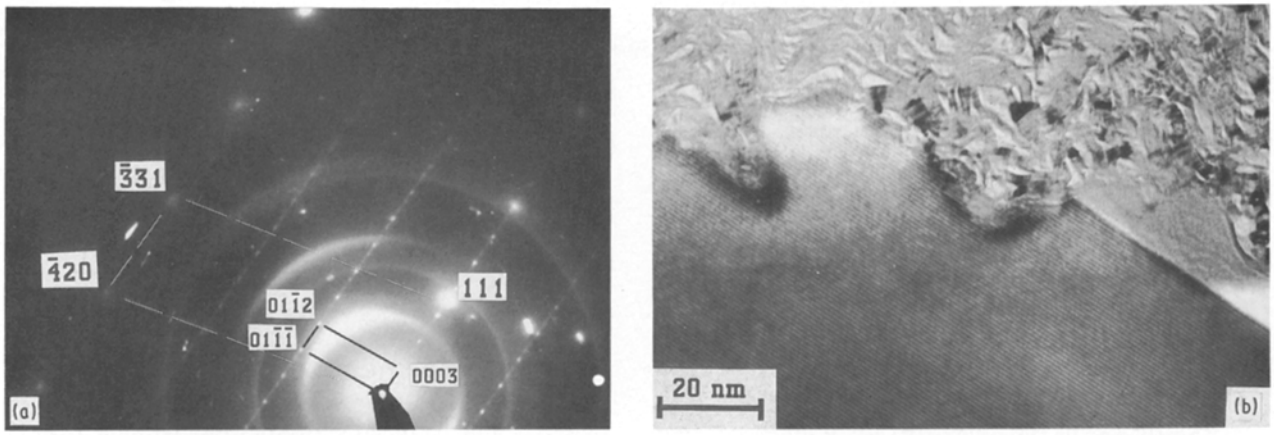


*Figure 7* (a) Indexed diffraction pattern showing orientation relationship between a carbide and the aluminium matrix. (b) Micrograph showing the area from which diffraction pattern was obtained. Note the highly convoluted graphite crystallites at the surface of the fibre.

(002) planes are parallel to the (0003) carbide planes.

## 4. Discussion

Considering firstly the tensile strength, this work has very clearly shown that it can be varied over a wide range simply by use of different fibres and by appropriate choice of the surface treatment. If the matrix alloy were also to be varied, a somewhat larger range of strength would be obtained [20]. Young's modulus is reasonably well predicted by the rule-of-mixtures, and is not significantly affected by surface treatments.

The shear test data of Tables II–IV show an increase in the composite shear strength as a result of surface treatment. As there was no major change in fracture surface morphology, and as the volume fraction and the matrix alloy are the same for all the composites in Tables II and III, the increase in composite shear strength must arise from an increase in interface shear strength resulting from improved fibre–matrix adhesion. It is noted from Table IV that, within a particular fibre–matrix system, the composite shear strength, $\tau_{cs}$, can be tripled by suitable surface treatment while the interfacial shear strength, $\tau_{int}$, can be increased more than five-fold. These properties can vary over a similarly wide range even without surface treatment depending on the choice of fibre (Table II). Furthermore, it should be noted that these tables show a consistent inverse relationship between composite longitudinal tensile strength and $\tau_{cs}$ or $\tau_{int}$.

It is clear from the XPS analysis that the surface treatments lead to an increase in the O/C ratio, and other workers have identified reactive groups such as carboxyl, hydroxyl and carbonyl groups at the fibre surface [21, 22]. Also, both chemical analysis of the interface and direct observation in the TEM reveal an increase in the amount of $Al_4C_3$ at the interface in surface-treated fibre-reinforced composites. It can be concluded therefore that the surface treatment leads to an increase in the chemical reaction at the interface which is accompanied by an increase in adhesion. The reasons for this increase are also shown by the TEM results.

Although generally highly oriented parallel to the fibre axis, the edge planes of the graphite crystallites are occasionally exposed at the fibre surface, exposing reactive sites which will rapidly chemisorb oxygen and form active groups on the fibre surface [15] as verified by the current XPS analysis. Fig. 6 shows that these crystallite edges can provide nucleation sites for aluminium carbides during and immediately after infiltration. The presence of the oxide groups on the fibre surfaces may catalyse the formation of $Al_4Cl_3$ or they may take no part in the reaction, but simply indicate that reactive sites are available. Any number of other speculative models could be advanced for the initiation reaction, but there currently exist no substantial data to support any of them.

Although the precise atomistic mechanism is still uncertain, it has been clearly shown that fibre-surface treatment leads to an increase in specific surface area, which may be qualitatively termed roughness. The scale of roughening is too small to be characterized by SEM, and must therefore be on the nanometre scale. Roughening on this scale would be sufficient to pit some of the highly convoluted graphite crystallites, and surface treatment thus exposes the reactive edges where they would not otherwise have been exposed. Consequently the number of reactive surface sites and, finally, of aluminium carbides, increases. The increase in reactivity between the aluminium and the fibre may contribute significantly to the increase in fibre–matrix adhesion found after surface treatment.

Yoon and Okura [12] recently reported seeing no direct correspondence between the graphite lattice and that of the aluminium carbide; however this is not surprising as the PAN-based fibres which they used contain very small crystallites. In the pitch-based fibres which we examined here, 15–20 % of the carbides exhibited the high degree of epitaxy with the graphite planes as illustrated in Fig. 6. Considering that the probability of locating the actual nucleation site is very small, such a large number of observations is certainly greater than would be made if the carbides were randomly nucleated.

It is proposed, therefore, that carbide formation is a conventional two-step nucleation and growth process

wherein nucleation occurs preferentially at the plane edges, but growth is constrained by the normal interfacial free energy, coherency and elastic stress considerations, so that it occurs most readily along certain planes and directions. Thus many nuclei are produced but only favourably oriented ones will grow. Furthermore, the nucleation sites are larger and more likely to give rise to a viable nucleus in the pitch-based fibres than in PAN-based fibres. The observation of a consistent matrix/carbide orientation relationship in this and in other work is thus a result of the preferred growth behaviour rather than preferred nucleation behaviour.

Nevertheless, as the fibres are only sparsely covered by the carbides, the majority of the fibre surface atoms must still bond to the aluminium matrix by low-energy interactions such as electrostatic; $\pi$-bonding; hydrogen bonding; or donor–acceptor interactions. Indeed, it would be remarkable if such a small volume fraction of carbides was able to 'key' the fibres and matrix together strongly enough to cause such marked increases in adhesion or interfacial shear strength. An alternative mechanism is that simple mechanical interactions between the matrix and the roughened fibre surface provide a major contribution to the increased interfacial shear strength.

With surface-treated fibres, increased fibre/matrix adhesion leads to a higher interfacial shear strength, but consequently reduces the ease of debonding. Hence stress concentrations develop and the so-called catastrophic failure mode occurs. Clearly a balance must be found where the interfacial shear strength is high enough to provide efficient load transfer, so that the fibres may be loaded to a significant fraction of their yield stress while still allowing debonding to occur at low enough stresses to relieve stress concentrations. A further possible reason for the decrease in composite tensile strength after surface treatment could be that the surface treatment leads to a decrease in fibre properties. This is certainly a contributing factor for the nitric acid M40 fibres, which have a 10 % reduction in tensile properties after surface treatment, but the magnitude of the composite strength degradation cannot be explained solely on this basis.

## 5. Conclusions

1. $Al_4C_3$ is the only reaction product at the interface. For identical processing conditions, the graphite crystallite size greatly influences the extent of carbide formation.
2. Oxidative surface treatment of carbon fibres leads to an increase in carbide concentrations at the interface.
3. Oxidative surface treatment of carbon fibres leads to an increase in surface roughness.
4. Increases in interfacial carbide concentration, surface roughness and number of exposed graphite crystallite edges all contribute to greatly increased interfacial shear strength in surface-treated composites.
5. The fibre–matrix adhesion in C/Al composites is mostly a low-energy interaction.
6. Carbide nucleation occurs preferentially at the edges of graphite crystallites.


## Acknowledgements

The authors gratefully acknowledge the provision of material and financial support from Honda R & D Co. Ltd, Japan, during the course of this work.


## References


1. D. HULL, "An Introduction to Composite Materials" (Cambridge University Press, Cambridge, 1981).
2. A. G. METCALFE and M. J. KLEIN, in "Composite Materials" Vol 1 edited by L. J. Broutman and R. H. Krock, (Addison-Wesley, Reading, MA, 1974) p. 125.
3. R. WU, in Proceedings of the Second International Conference on Composite Interfaces, Cleveland, OH, edited by H. Ishida, June 1988, (Elsevier, NY, 1988) p. 43.
4. H. NAYEB-HASHEMI and J. SEYYEDI, *Metall. Trans. A* **20A** (1989) 727.
5. M. F. AMATEAU, *J. Compos. Mater.* **10** (1976) 279.
6. X. CHEN and G. HU, in Proceedings of the Second International Conference on Composite Interfaces, edited by H. Ishida, June 1988, p. 381.
7. L. D. BROWN, C. L. GROVE and H. L. MARCUS, in Proceedings of a Conference on Interfaces in Metal Matrix Composites, New Orleans, Lousiara, edited by A.K.Dhingra and S. G. Fishman, TMS-Annual Meeting, March 1986, (TMS-AIME, Warrendale, PA, 1986) p. 205.
8. M. VEDULA and R. A. QUEENEY, *ibid.* p. 227
9. I. H. KHAN, *Metall. Trans. A.* **7A** (1976) 1281.
10. G. BLANKENBURGS, *J. Aus. Inst. Metals* **14** (1969) 236.
11. W. C. HARRIGAN, Jr., *Metall. Trans. A.* **9A** (1978) 503.
12. H-S. YOON and A. OKURA, *SAMPE J.* **26** (1990) 19.
13. G. DOREY, *J. Phys. D: Appl. Phys.* **20** (1987) 245.
14. D. J. JOHNSON, *ibid.* **20** (1987) 286.
15. E. FITZER, "Carbon Fibers and Their Composites" (Springer, Berlin, 1985).
16. E. ZYWICZ and D. M. PARKS, *Compos. Sci. Technol.* **33** (1988) 295.
17. "In Plane Shear Strength of Reinforced Plastics", ASTM Standard D3846-79 (ASTM, Philadelphia, PA).
18. S. OCHIAI and K. OSAMURA, in Proceedings of the Second International Conference on Composite Interfaces, Cleveland OH, edited by H. Ishida, June 1988, (Elsevier, NY, 1988) p. 413.
19. M. K. SHOSHOROV, L. E. GUKASIAN and L. M. USTINOV, *J. Compo. Mater.* **17** (1983) 527.
20. A. P. DIWANJI, PhD thesis, University of Delaware, 1990
21. T. TAKAHAGI and A. ISHITANI, *Carbon* **22** (1984) 43.
22. J.-B. DONNET, *ibid.* **6** (1968) 161.



*Received 7 January*
*and accepted 7 June 1991*